RESEARCH ARTICLE

Analytical model of friction behavior during polymer scratching with conical tip

Chengkai JIANG, Han JIANG*, Jianwei ZHANG, Guozheng KANG

Applied Mechanics and Structure Safety Key Laboratory of Sichuan Province, School of Mechanics and Engineering, Southwest Jiaotong University, Chengdu 610031, China

Abstract: To investigate the effects of the contact geometry, interfacial friction, and substrate recovery on the behavior of polymer scratching using a conical tip, an analytical model is proposed. The normal stress acting on the contact surface between the tip and the substrate is described as a function of the included angle θ, representing the angle between two planes across the axis of the conical tip, and the attack angle β, representing the angle between the conical surface and the substrate material surface. The effects of the rear contact geometry on the scratch friction between the tip and substrate, represented by recovery angle φ, owing to the instantaneous elastic recovery of the polymer substrate, are also introduced. Validated by the experimental and numerical results from the literature, the proposed analytical model can describe well the scratch coefficient of friction (SCOF), which is defined as the ratio of the tangential force to the normal force. Meaningful guidance is provided to understand the scratch friction behavior.

Keywords: polymer scratch; contact geometry; elastic recovery; scratch coefficient of friction

1 Introduction

Owing to their relatively poor mechanical properties, polymeric materials can easily be scratched, and the surface damage from such scratches will change/weaken the morphology, functionality, and aesthetics of the original surface. It is well known that the adhesive behavior between the tip and substrate significantly affect the polymer scratch behavior. To evaluate the scratch resistance of a polymer, the single-pass test with a hard scratch tip has been widely adopted [1–6]. Many scratch experiments have been conducted for different polymers and their micro-/nano-composites [7–14]. Various scratch damage patterns have also been observed [2, 8–13].

A finite element (FE) analysis was also conducted to study the scratch damage mechanisms, as well as the influence of the material properties and/or contact conditions on the scratch behavior [15–24]. For instance,

Jiang et al. [15] found that the scratch performance of polypropylene (PP) improves with a decrease in interfacial friction when using the FE method. Pelletier et al. [16] numerically demonstrated that the interfacial friction significantly affects the real contact area between the scratch tip and polymethylmethacrylate (PMMA) substrate. Feng et al. [23, 24] considered the combined Coulomb and plastic friction effect to study the impact of the yield strength on the scratch friction behavior.

Considering the complex contact condition between the scratch tip and substrate, necessary assumptions are needed when establishing an analytical model. For scratch friction with a conical tip, Subhash and Zhang [25] assumed the normal stress applied to a contact surface as a constant value, which was an oversimplification. Lafaye et al. [26–28] established an analytical model and explored three forms of normal stress distribution. Komvopoulos [29] established an analytical model for a conical tip with a spherical

---

* Corresponding author: Han JIANG, E-mail: jianghan@home.swjtu.edu.cn

extremity sliding on a rigid-perfectly-plastic material. Jardret et al. [30] studied the use of a Berkovich tip. Tayebi et al. [31] investigated a spherical tip, and Briscoe et al. [32] studied a conical tip. Most of these works assumed that the contact only exists between the frontal half of the scratch tip and the substrate. Based on an *in-situ* observation of the scratch experiment, Gauthier et al. [33, 34] found that the substrate instantaneously recovers after the tip passes by. The contact between the rear part of the scratch tip and recovered substrate is observed, which should be considered to establish a comprehensive analytical model of the scratch behavior. Bucaille et al. [35] extended the model of Goddard and Willman [36] to describe the rear contact between a conical tip and an elastic–perfect plastic material as a frictionless case. Lafaye et al. [37, 38] further developed this using a conical tip, a spherical tip, and a conical tip with a blunted spherical extremity. They found that the effects of the instantaneous elastic recovery of the substrate on the scratch behavior cannot be neglected.

In this paper, an analytical model is proposed to study the scratch friction behavior of a conical tip-polymer substrate system. Because of the viscoelastic nature of a polymer, a theoretical description of the scratch friction is not easy to achieve. To analyze the local interaction between the tip and substrate, the substrate material is assumed as an elastic–plastic material without strain hardening. First, the normal stress distribution on the contact surface between the tip and substrate is explicitly defined as a function of the included angle θ and attack angle β. The elastic recovery of the substrate is also included. After validation based on experimental and numerical results from the literature [21, 25, 35, 39], the proposed analytical model is utilized to thoroughly investigate the influences of the contact geometry, interfacial friction, and substrate recovery on the scratch friction.

2 Theoretical model

The scratch coefficient of friction (SCOF), also called the apparent friction coefficient [26–28], or overall friction coefficient [25, 39], is defined in Eq. (1) as the ratio between the tangential force F_T and the normal force F_N exerted on the scratch tip, as schematically shown in Fig. 1(a).

$$\mu_{SCOF} = \frac{F_T}{F_N} \tag{1}$$

2.1 Subhash and Zhang (S&Z) model

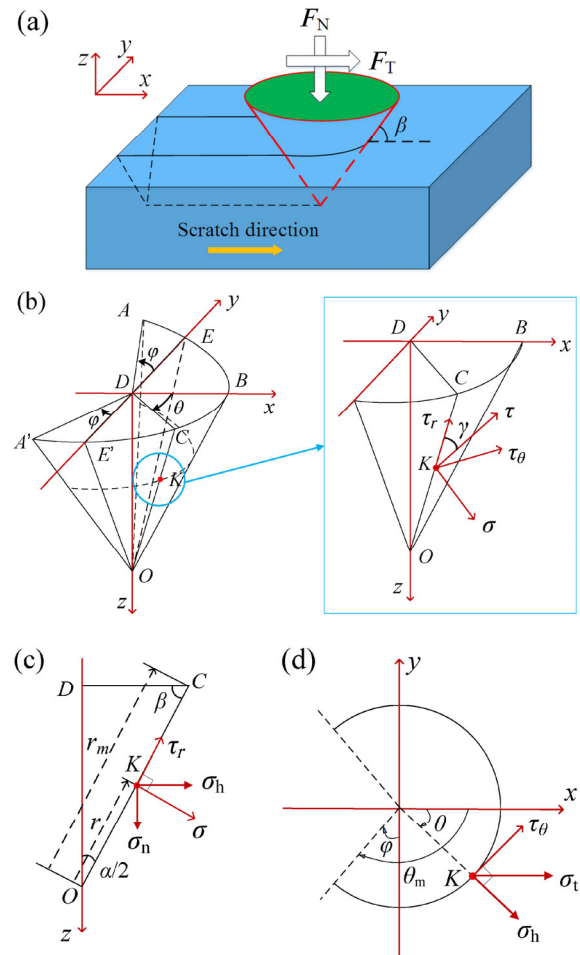Subhash and Zhang [25] proposed an analytical model

Fig. 1 (a) 3D view of the conical tip-substrate scratch; (b) schematic of the contact surface and stress components at point K; (c) the stress components at point K from side view; (d) the stress components at point K from top view. Here, α is the conical apex angle; OD is the axis of conical tip; DB is the radius of the circle on the top contact surface; θ is the included angle between planes OCD and OBD. r is the length of OK. σ is the normal stress on contact surface (on plane *OCD* and perpendicular to *OC*). τ is the tangential stress on contact surface following the material flow direction at K. $\gamma = \eta\theta$ is the angle between τ and OC. τ_r is along OC and τ_θ is perpendicular to OCD. The σ_h is the stress component of σ (on plane OCD and perpendicular to OD). θ_m is the maximum included angle. σ_t and σ_n are the resulting stresses at point K along the scratch direction and the axial direction, respectively.

to study the scratch behavior using a conical tip. In their work, the SCOF is written as

$$\mu_{\text{SCOF}} = \frac{\sin\beta - \dfrac{\mu_{\text{s}}(\eta + \cos\beta)}{\eta^2 - 1} \cdot \cos\left(\dfrac{\eta\pi}{2}\right)}{\dfrac{\pi}{2} \cdot \cos\beta - \dfrac{\mu_{\text{s}} \cdot \sin\beta}{\eta} \cdot \sin\left(\dfrac{\eta\pi}{2}\right)} \quad (2)$$

where β is the attack angle, which represents the angle between the conical surface and the substrate material surface, η is a parameter to characterize the material flows on the contact surface, and μ_{s} is the local interfacial friction coefficient. All variables are illustrated in Fig. 1. Assuming that the distribution of normal contact stress is independent of the included angle θ, they obtained a constant value of the normal stress σ along any arbitrary cross-section on the contact surface, as schematically shown in Fig. 2(b). For this oversimplified situation, the S&Z model provides a fair prediction of the scratch performance for cases in which both β and μ_{s} are small.

However, the effects of other important geometric factors, such as the conical apex angle α, on the normal
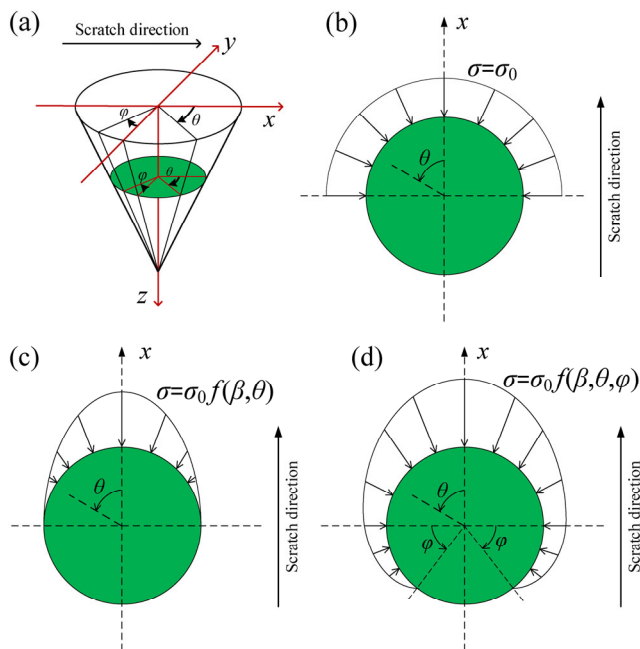

Fig. 2 Schematic of the normal stress distribution on one horizontal cross-section of the contact surface: (a) 3D illustration of conical tip; (b) the S&Z model; the proposed model (c) without elastic recovery and (d) with elastic recovery. θ is the included angle. φ is the recovery angle representing the rear contact between tip and substrate.

contact stress are not included in the above model. In addition, their work assumed that contact only exists between the frontal half of the scratch tip and the substrate, i.e., $\theta \in [0, \pi/2]$, which completely neglects the elastic recovery of the polymer substrate at the rear contact.

2.2 Proposed model

The effects of the contact geometry and the elastic substrate recovery on the contact normal stress between the scratch tip and underneath part of the substrate are taken into consideration in the present study.

2.2.1 Effects of geometric factors on normal contact stress

The normal stress on the contact surface between the tip and substrate is correlated with the tip geometry, the mechanical properties of the substrate, and the adhesive behavior of the contact pair. For conical tip scratching, the normal stress distribution on the horizontal cross-section, with different heights, of the contact surface should follow the same tendency. In this work, two geometrical factors, i.e., the included angle θ and the attack angle β, were separated and explicitly considered to study the scratch friction behavior. Without a loss of generality, the normal stress acting on the contact surface line of one horizontal cross-section of the conical tip, as a function of many factors, namely, $\sigma = \sigma(\theta, \beta, r, \cdots)$, may be simplified as

$$\sigma = \sigma(r, \cdots)f(\theta, \beta) \quad (3)$$

Here, $\sigma(r, \cdots)$, written as σ_0 [25], may change with the location of the horizontal cross-section but remain constant at the same cross-section (see Fig. 2(b)). In addition, $f(\theta, \beta)$ is a function of the included angle θ and attack angle β.

Because the substrate material flowing on one horizontal cross-section of the contact surface is phenomenologically similar to the fluid uniformly flowing around the circular cylinder, $f(\theta, \beta)$ can be presented in a form similar to the distribution of the fluid pressure on the cylinder surface [40], that is,

$$f(\theta, \beta) = 1 - \sin^2 \xi\beta\theta \quad (4)$$

The parameter ξ is discussed in Section 2.2.2. Whereas the S&Z model assumes that the normal

contact stress is independent of θ and β, Eqs. (3) and (4) explicitly include the effects of θ and β on the normal stress distribution, which is described in Figs. 2(c) and 3.

As illustrated in Fig. 3(a), the tangential and normal projection contact areas depend on β. When $\beta = 0°$, the conical tip converts into a flat punch. Thus, the contact pair has a face-to-face contact, as shown in Fig. 3(b). In this case, the normal stress distribution of the proposed model (the solid black line in Fig. 4) is found to be same as in the S&Z model (the red square in Fig. 4). Even for other scratch tips, of which β is not equal to zero, the difference between the two models may be ignored if the attack angle is small. For instance, for $\beta = 20°$, the maximum difference between the proposed (the dashed green line in Fig. 4) and S&Z models (the red square in Fig. 4) is less than 10%.

However, for a larger β, the difference has to be considered. For an extreme case with $\beta = 90°$, the shape of the conical tip emerges into a "needle-like" shape (as shown in Fig. 3(c)). The maximum normal
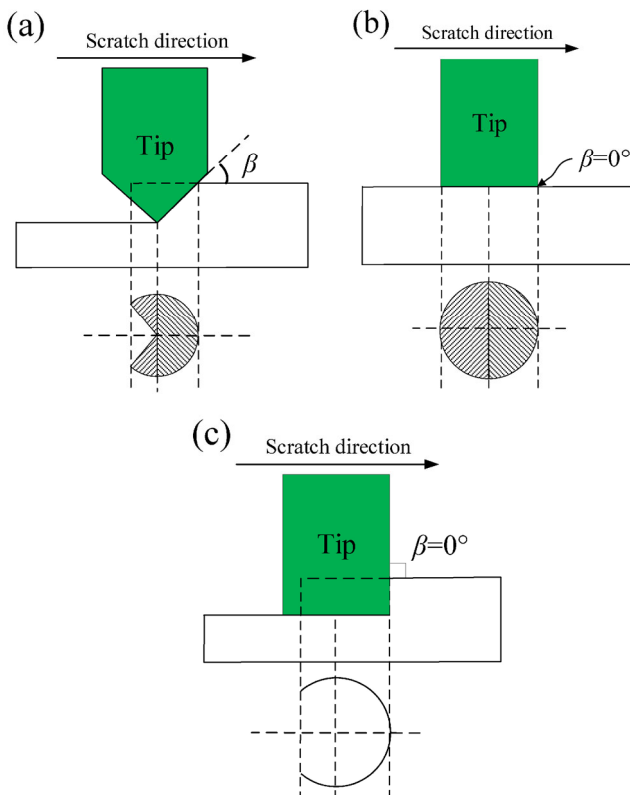

Fig. 3 Schematic of the conical tip-polymer substrate systems with different attack angle β: (a) $0° < \beta < 90°$, (b) $\beta = 0°$, and (c) $\beta = 90°$.
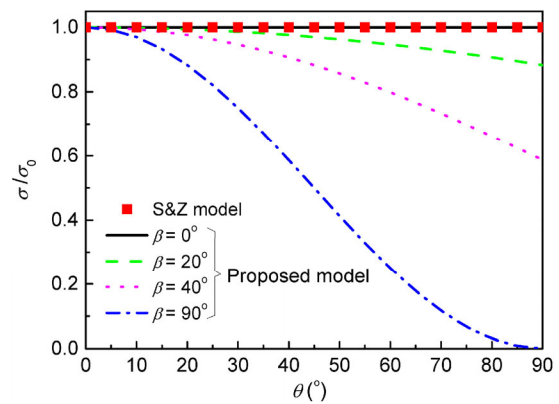

Fig. 4 Normal contact stress as a function of the included angle θ with a zero-recovery angle.

stress appears at the location of $\theta = 0$, as shown in Fig. 2(c), and then gradually decreases toward zero at the edge of the contact area. As indicated in Fig. 4, this phenomenon can be described through the proposed model but not by the S&Z model.

2.2.2 Effects of substrate recovery on normal contact stress

As revealed in the literature [32–37], the significant influence of the substrate's elastic recovery has to be included. The resultant contact force existing on the rear half of the scratch tip actually pushes forward. As shown in Fig. 2(d), the recovery angle $\varphi \in [0, \pi/2]$ on the rear half of the contact surface is adopted to characterize the extent of the elastic recovery of the substrate. The included angle θ changes to

$$\theta \in \left[0, \frac{\pi}{2} + \varphi \right] \tag{5}$$

where φ indicates the recovery angle. If $\varphi = 0$, then we go back to case (c) or (b) of Fig. 2.

From the extreme case in which the normal stress at the edge of the contact surface is zero when $\beta = 90°$, as shown in Fig. 3(c), we obtain the following:

$$\sigma \big|_{\theta = \frac{\pi}{2} + \varphi, \beta = \frac{\pi}{2}} = 0,$$

$$\xi = \frac{2}{\pi + 2\varphi} \tag{6}$$

The SCOF can then be formulated under consideration of the effect of the substrate recovery, contact geometry, and interfacial friction, namely,

$$\mu_{\text{SCOF}} = \frac{A - B\mu_{\text{S}}}{C - D\mu_{\text{S}}} \qquad (7)$$

Here, A and C are functions of φ and β, and B and D are functions of η, φ, and β. The detailed derivation of Eq. (7) of the proposed model can be found in the Appendix, where the computational details of the corresponding A, B, C, and D are also provided.

3 Results and discussion

The SCOFs calculated using the proposed and S&Z models, as well as obtained from the experimental data in the literature, are compared. In Sections 3.1 and 3.2, we discuss the effects of the contact geometry and interfacial friction, respectively, on the SCOF under a zero-recovery angle, $\varphi = 0°$. In addition, the influence of the substrate recovery on the SCOF is discussed in Section 3.3.

3.1 Effects of contact geometry on the SCOF

The tangential scratch friction force consists of two components, i.e., the interfacial friction between the contact pair and the resistance from the deformed substrate material [25–28]. In an extreme case of $\beta = 0°$, i.e., when the conical tip has a 180° apex angle, as shown in Fig. 3(b), a face-to-face contact is found between the contact pair. The material flow on the contact surface is expected to be parallel to the scratch direction. Thus, the flow line parameter can be taken as $\eta = 1$. Then, the SCOFs of both analytical models are reduced as $\mu_{\text{SCOF}} = \mu_{\text{S}}$, and the substrate deformation-induced resistance disappears.

For an idealistic case in which $\mu_{\text{S}} = 0$, the tangential resistance comes only from the deformation of the substrate material. Whereas the S&Z model over simplifies μ_{SCOF} as $\dfrac{2}{\pi}\tan\beta$, Eq. (7) reduces to

$$\mu_{\text{SCOF}} = \frac{\tan\beta\left[1 + \cos(2\beta)\middle/\left(1 - \left(\dfrac{4}{\pi}\beta\right)^2\right)\right]}{\dfrac{\pi}{2} + \dfrac{\pi}{4\beta}\cdot\sin(2\beta)} \qquad (8)$$

Eq. (8) converges to $\dfrac{2}{\pi}\tan\beta$ while $\beta \to 0°$. This implies

that the S&Z model is a good approximation for a small attack angle. However, for a large attack angle, the proposed model should be utilized to describe the SCOF.

Ducret et al. [39] conducted scratch tests on UHMWPE under different constant normal loads with four attack angles, i.e., 15°, 30°, 45°, and 60°. The SCOFs from their experimental work, as well as from both analytical models, are plotted in Fig. 5. It is clear that, whereas the results from both analytical models agree well with the experimental data for a small attack angle β, the proposed analytical model provides a better prediction for cases with a large β. It should be noted that the value of μ_{s} used in both analytical models here is 0.03 [41–43].

3.2 Effects of interfacial friction on the SCOF

Figure 6 shows the contours of the SCOF as the function of η and μ_{s} at two attack angles, i.e., $\beta = 10°$ and 60°, respectively. It is not surprising that, for a small attack angle, little difference is found between the two analytical models (as illustrated in Fig. 6(a)). However, for a large attack angle (Fig. 6(b)), the SCOF predicted by the proposed model is larger than that by the S&Z model, and the difference (14%–36% for various values of η and μ_{s}) cannot be ignored.

It can also be seen from Fig. 6 that, for a given η, the SCOF increases with an increase in μ_{s}, and it increases more rapidly for a larger attack angle than a smaller one. The reason for this phenomenon is that,
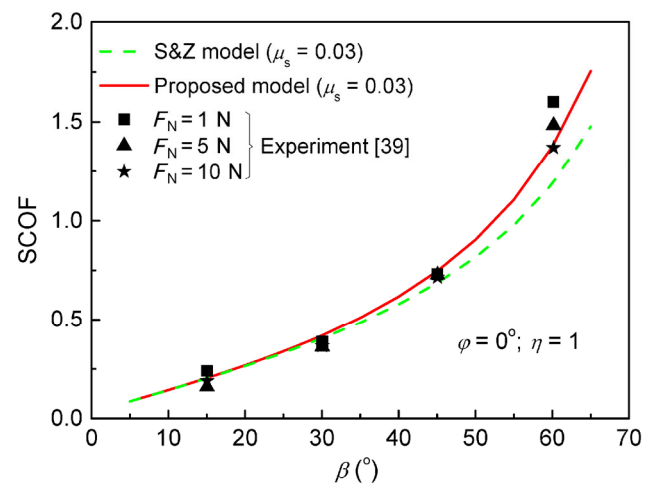

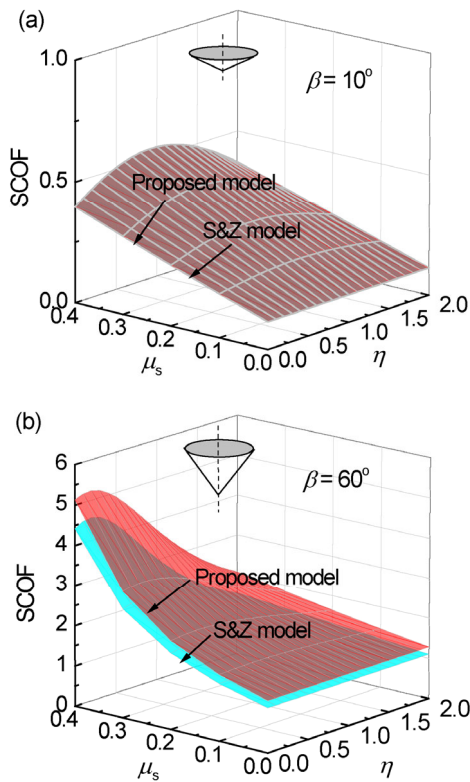**Fig. 5** SCOFs with a zero-recovery angle as a function of β.

Fig. 6 SCOFs of the conical tip-polymer substrate systems with a zero-recovery angle: (a) $\beta = 10°$ and (b) $\beta = 60°$.

whereas the friction-induced resistance dominates the scratch friction for a small attack angle β, the substrate deformation has a greater contribution to the scratch resistance for a large β.

Felder et al. [21] numerically investigated a conical tip scratch for an elastic–perfect-plastic material with a small attack angle ($\beta = 19.7°$) when ignoring the recovery angle φ. The authors took the interfacial friction coefficient to be 0, 0.05, 0.1, 0.15, and 0.2, respectively. The SCOFs of different values of μ_s from their numerical work and the two analytical models are shown in Fig. 7(a). It is clear that both analytical models show good agreement with Felder's work [21] when the attack angle is small.

Meanwhile, for large attack angles ($\beta = 45°$ and $60°$), the predicted SCOFs of both analytical models are compared with the numerical results [25], as plotted in Fig. 7(b). For a comparison with the results of the S&Z model [25], η is chosen as 3/2 and 4/3 for $\beta = 45°$ and $60°$, respectively. This shows that the proposed model provides a more accurate SCOF than the S&Z model.
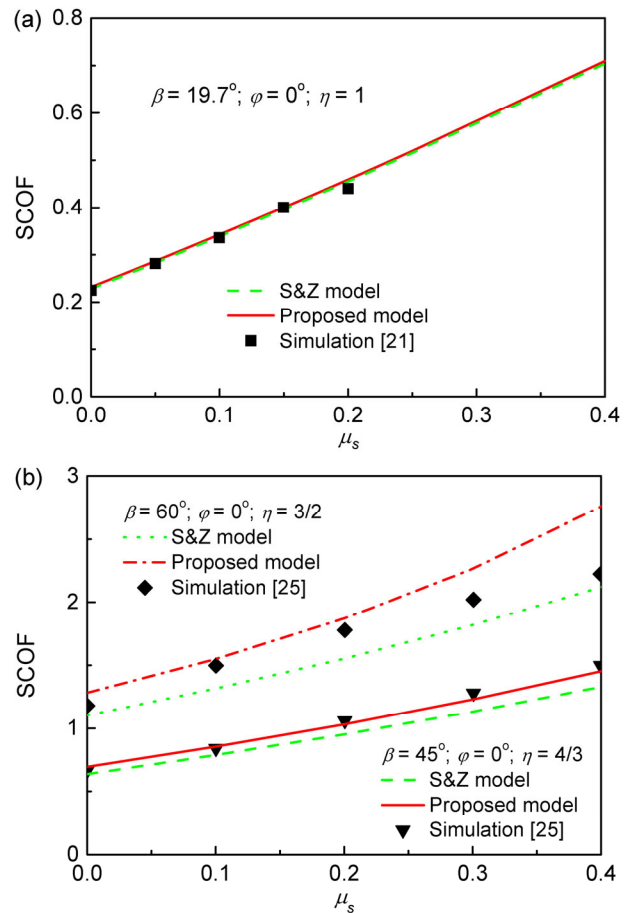

Fig. 7 SCOFs (ignoring the substrate recovery) as a function of μ_s: (a) $\beta = 19.7°$, (b) $\beta = 45°$ and $60°$.

3.3 Effects of the substrate recovery on the SCOF

Gauthier and Schirrer [33, 34] conducted *in-situ* observations of the polymer scratch process. They found that an instantaneous recovery of the substrate material, after the tip passes by, will create contact with the rear part of the scratch tip. Thus, an additional resultant forward pushing force is applied at the tip. The substrate elastic recovery shows an important influence as can be phenomenologically determined from Fig. 2(d). A small change in the recovery angle φ may have a significant influence on the SCOF.

In the proposed model, the normal contact stress distribution, σ/σ_0, is correlated with the included angle θ, the attack angle β, and the recovery angle φ. The contours of the normal contact stress with different recovery angles are plotted in Fig. 8. For a given β, σ/σ_0 converges monotonically from its minimum value to 1 if θ decreases from θ_m to 0°. Similarly,
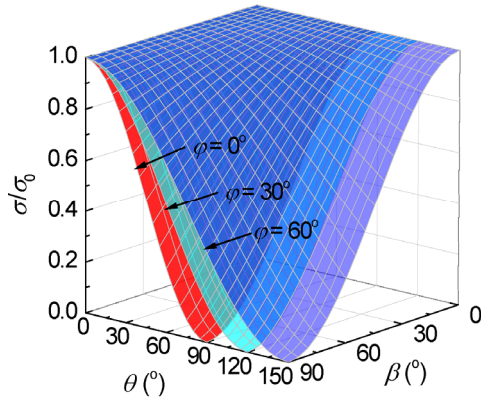
Fig. 8 Effect of the elastic recovery on the contact normal stress (θ is the included angle; β is the attack angle).

σ/σ_0 is found to increase to 1 if β reaches 0°. For the case of a small β and small θ, σ/σ_0 is very close to 1, which will converge to a perfectly elastic contact. For a similar shape, a larger contact area on the rear half of the tip will induce a larger forward pushing force.

For two attack angles, i.e., $\beta = 10°$ and 60°, the contour planes of SCOF with different substrate recovery angles ($\varphi = 0°$, 30°, and 60°) are shown in Fig. 9. When the overall shape of the contour planes

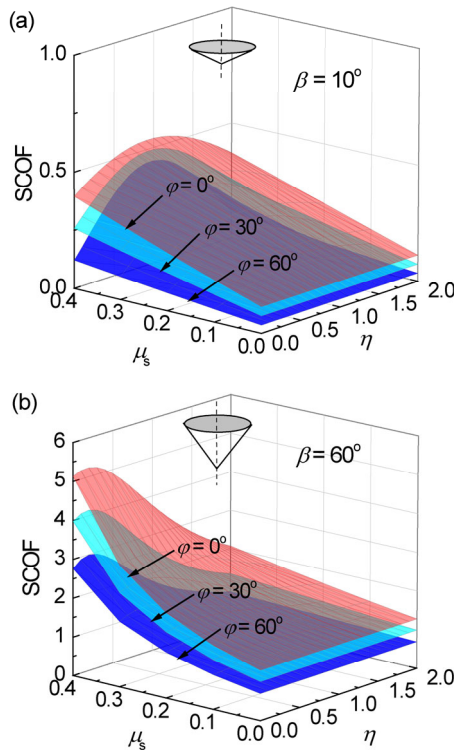**Fig. 9** Effect of the elastic recovery on SCOFs: (a) $\beta = 10°$ and (b) $\beta = 60°$.

of the SCOF remains similar for various attack angles, the recovery angle can clearly reduce the SCOF regardless of the attack angle. For $\beta = 10°$, the maximum relative differences in the SCOF between $\varphi = 0°$ and $\varphi = 30°$, 60° reach 35.75% and 69.78%, respectively. The maximum relative differences reach 35.16% and 57.84%, respectively for $\beta = 60°$.

From the illustrations of the two tips (see Figs. 9(a) and 9(b), respectively), it can be seen that, for a small attack angle, such as $\beta = 10°$ in Fig. 9(a), in which the conical tip is very close to a flat punch, the SCOF is dominated by the interfacial friction. However, for a large attack angle, such as $\beta = 60°$ in Fig. 9(b), the deformation resistance of the substrate also has a significant contribution to the SCOF. Thus, the SCOF becomes larger.

Bucaille et al. [35] conducted a numerical simulation of a frictionless scratching of an elastic–perfect-plastic substrate using a conical tip with an attack angle of $\beta = 19.7°$. They obtained the SCOFs corresponding to various elastic recovery angles. In the extreme case of $\mu_s = 0$, the proposed model is reduced to $\mu_{\mathrm{SCOF}} = A/C$, which is a function only related to β and φ, whereas the S&Z model is reduced to a function related only to β. It is found that η shows no influence on the SCOF for either model. The SCOFs, as a function of the recovery angle, obtained from the proposed analytical model and the numerical simulation results [35], along with a constant value from the S&Z model, are given in Fig. 10. It is clear that the influence of the recovery angle described by the proposed analytical model agree well with the literature [35], whereas the S&Z model is not capable of this because no elastic recovery is included.
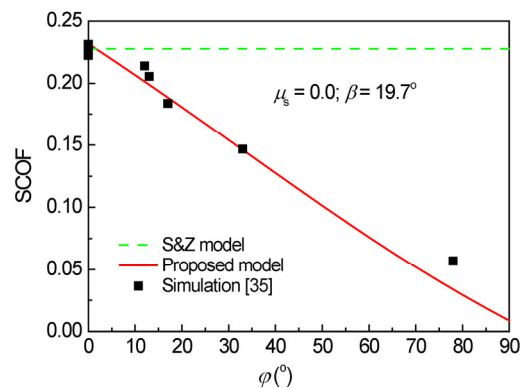

Fig. 10 SCOFs as a function of φ.

It should be noted that the material pile-up in front of the scratch tip, commonly observed during the scratch process, has yet to been considered for the proposed analytical model. It is also known that the substrate recovery is closely correlated with the material properties such as the elastic modulus, yield strength [21, 23], and viscoelastic characteristic [44–48], as well as the possible influence of the crystallinity on these properties [49], which are inherently important for the scratch friction performance of polymeric materials. A comprehensive analytical investigation of polymer scratching should be further conducted when considering the above factors.

4   Summary

In this paper, an analytical model is proposed to investigate the effects of the contact geometry, the interfacial friction, and the substrate elastic recovery on the scratch performance for a conical tip-polymer substrate system. The following conclusions were drawn:

(1) For a small attack angle, the proposed analytical model is somewhat close to the S&Z model. For a large attack angle, the effects of the contact geometry, i.e., the included angle θ and the attack angle β, can be described more accurately using the proposed model.

(2) Validated through experimental and numerical studies, the proposed analytical model can describe well the scratch behavior with a consideration of the contact geometry, interfacial friction, and substrate elastic recovery.

(3) The proposed analytical model provides meaningful guidance to understanding the scratch friction behavior when using a conical tip.

Acknowledgements

Appendix

A three-dimensional diagram of conical tip scratching on a polymer substrate is schematically depicted in Fig. 1(a). We assume a perfect contact between the conical tip and the polymer substrate in the proposed model. The contact surface, with all necessary variables established in the Cartesian coordinates, is shown in Fig. 1(b). The conical apex angle is defined as α. Line OD is the axis of the conical tip, and its length, d, is the instantaneous indentation depth of the tip. Line DB is the radius of the circle on the top contact surface, and its direction is in accordance with the scratch direction. The angle θ represents the included angle between planes OCD and OBD, and an arbitrary chosen point K located on line OC on the contact surface has a distance of r from the original point O. During the scratch process, at point K, the normal and tangential stresses are denoted by σ and τ, respectively. Here, a simple formulation is given as

$$\tau = \mu_s \sigma \tag{A1}$$

where μ_s is the local friction coefficient on the contact surface. The normal stress σ is perpendicular to line *OC* toward the outside of the conical surface located on plane OCD. The direction of τ coincides with the material flow direction at K. The angle between τ and line OC is defined as $\gamma = \eta\theta$, as shown in Fig. 1(b), where parameter η is utilized to characterize the material flows around the scratch tip. For simplicity, the tangential stress τ is decomposed into τ_r along the line OC and τ_θ perpendicular to the plane OCD, respectively (see Fig. 1(b)). Therefore, we have

$$\begin{cases} \tau_r = \tau\cos\gamma = \tau\cos(\eta\theta) \\ \tau_\theta = \tau\cos\gamma = \tau\sin(\eta\theta) \end{cases} \tag{A2}$$

At point K, as schematically shown in Figs. 1(c) and 1(d), the resulting stresses exerted on the scratch tip along the scratch direction σ_t and the axial direction σ_n are respectively

$$\begin{cases} \sigma_t = (\sigma\sin\beta + \tau_r\cos\beta)\cos\theta + \tau_\theta\sin\theta \\ \sigma_n = \sigma\cos\beta - \tau_r\sin\beta \end{cases} \tag{A3}$$

Substituting Eqs. (A1) and (A2) into Eq. (A3), we obtain

$$\begin{cases} \sigma_t = \sigma\left[\left(\sin\beta + \mu_s\cos(\eta\theta)\cos\beta\right)\cos\theta + \mu_s\sin(\eta\theta)\sin\theta\right] \\ \sigma_n = \sigma\left(\cos\beta - \mu_s\cos(\eta\theta)\sin\beta\right) \end{cases}$$

(A4)

Finally, the total tangential force F_T and normal force F_N applied on the scratch tip can be calculated by integrating σ_t and σ_n over the entire contact surface, respectively. The contact surface is symmetric about the x-z plane, as shown in Fig. 1(b). In this work, only one-half of the contact surface (i.e., surface OA'E'B or OAEB in Fig. 1(b)) is utilized in the integration. Therefore,

$$\begin{cases} F_T = 2\int \sigma_t \mathrm{d}S = 2\cos\beta \int_0^{\theta_m}\int_0^{r_m} \sigma_t r\mathrm{d}\theta\mathrm{d}r \\ F_N = 2\int \sigma_n \mathrm{d}S = 2\cos\beta \int_0^{\theta_m}\int_0^{r_m} \sigma_n r\mathrm{d}\theta\mathrm{d}r \end{cases}$$

(A5)

where $\theta_m = \pi/2 + \varphi$ is the maximum included angle, and $r_m = d/\sin\beta$ is the length of line OC.

Substituting Eqs. (3) and (A4) into Eq. (A5), we obtain

$$\begin{cases} F_T = 2\cos\beta \int_0^{\theta_m}\int_0^{r_m} \sigma_0 f(\theta,\beta)\big[\left(\sin\beta \\ \quad + \mu_s\cos(\eta\theta)\cos\beta\right)\cos\theta + \mu_s\sin(\eta\theta)\sin\theta\big]r\mathrm{d}\theta\mathrm{d}r \\ F_N = 2\cos\beta \int_0^{\theta_m}\int_0^{r_m} \sigma_0 f(\theta,\beta)\big(\cos\beta \\ \quad - \mu_s\cos(\eta\theta)\sin\beta\big)r\mathrm{d}\theta\mathrm{d}r \end{cases}$$

(A6)

Further, Eq. (A6) can be written as

$$\begin{cases} F_T = 2\cos\beta\left(\int_0^{\theta_m} f(\theta,\beta)\big[\left(\sin\beta + \mu_s\cos(\eta\theta)\cos\beta\right)\cos\theta \\ \quad + \mu_s\sin(\eta\theta)\sin\theta\big]\mathrm{d}\theta\right)\left(\int_0^{r_m}\sigma_0 r\mathrm{d}r\right) \\ F_N = 2\cos\beta\left(\int_0^{\theta_m} f(\theta,\beta)\big(\cos\beta \\ \quad - \mu_s\cos(\eta\theta)\sin\beta\big)\mathrm{d}\theta\right)\left(\int_0^{r_m}\sigma_0 r\mathrm{d}r\right) \end{cases}$$

(A7)

Substituting Eq. (A7) into Eq. (1), the SCOF becomes

$$\mu_{SCOF} = \frac{\int_0^{\theta_m} f(\theta,\beta)\big[\left(\sin\beta + \mu_s\cos(\eta\theta)\cos\beta\right)\cos\theta + \mu_s\sin(\eta\theta)\sin\theta\big]\mathrm{d}\theta}{\int_0^{\theta_m} f(\theta,\beta)\big(\cos\beta - \mu_s\cos(\eta\theta)\sin\beta\big)\mathrm{d}\theta}$$

(A8)

Then, substituting Eq. (4) into Eq. (A8), the SCOF is written as

$$\mu_{SCOF} = \frac{A - B\mu_s}{C - D\mu_s}$$

(A9)

where

$A = \sin\beta\int_0^{\theta_m}\left(f(\theta,\beta)\cdot\cos\theta\right)\mathrm{d}\theta$,

$B = -\int_0^{\theta_m} f(\theta,\beta)\big(\cos\eta\theta\cos\beta\cos\theta + \sin\eta\theta\sin\theta\big)\mathrm{d}\theta$,

$C = \cos\beta\int_0^{\theta_m} f(\theta,\beta)\mathrm{d}\theta$,

and $D = \sin\beta\int_0^{\theta_m}\left(f(\theta,\beta)\cos\eta\theta\right)\mathrm{d}\theta$.

The derivation details of A, B, C, and D are shown in the following.

(i) Computation of the integral of A

$$A = \sin\beta\int_0^{\theta_m}\left(f(\theta,\beta)\cdot\cos\theta\right)\mathrm{d}\theta$$
$$= \sin\beta\int_0^{\theta_m}\cos\theta\mathrm{d}\theta + \sin\beta\int_0^{\theta_m}\cos(2\xi\beta\theta)\cos\theta\mathrm{d}\theta,$$

where the integrals of $\int_0^{\theta_m}\cos\theta\mathrm{d}\theta$ and $\int_0^{\theta_m}\cos(2\xi\beta\theta)\cdot\cos\theta\mathrm{d}\theta$ are respectively

$$\int_0^{\theta_m}\cos\theta\mathrm{d}\theta = \sin\theta_m = \sin\left(\frac{\pi}{2}+\varphi\right) = \cos\varphi$$

and

$$\int_0^{\theta_m}\cos(2\xi\beta\theta)\cos\theta\mathrm{d}\theta$$
$$= \frac{1}{2}\int_0^{\theta_m}\big[\cos(2\xi\beta\theta-\theta) + \cos(2\xi\beta\theta+\theta)\big]\mathrm{d}\theta$$
$$= \frac{1}{2}\cdot\frac{1}{2\xi\beta-1}\cdot\sin(2\xi\beta\theta_m-\theta_m)$$
$$\quad + \frac{1}{2}\cdot\frac{1}{2\xi\beta+1}\cdot\sin(2\xi\beta\theta_m+\theta_m)$$
$$= -\frac{1}{2}\cdot\frac{\cos(\varphi-\pi\xi\beta-2\xi\beta\varphi)}{2\xi\beta-1} + \frac{1}{2}\cdot\frac{\cos(\varphi+\pi\xi\beta+2\xi\beta\varphi)}{2\xi\beta+1}.$$

Substituting the integrals of $\int_0^{\theta_m}\cos\theta\mathrm{d}\theta$ and $\int_0^{\theta_m}\cos(2\xi\beta\theta)\cos\theta\mathrm{d}\theta$ into A, we obtained

$$A = \sin\beta\cos\varphi + \frac{1}{2}\sin\beta\cdot\left(\frac{\cos(\varphi-\pi\xi\beta-2\xi\beta\varphi)}{1-2\xi\beta}\right.$$
$$\left. + \frac{\cos(\varphi+\pi\xi\beta+2\xi\beta\varphi)}{2\xi\beta+1}\right)$$

$$= \left[\cos\varphi + \frac{\cos\varphi\cos(\pi\xi\beta + 2\xi\beta\varphi) + 2\xi\beta\sin\varphi\sin(\pi\xi\beta + 2\xi\beta\varphi)}{1 - 4\xi^2\beta^2} \right] \sin\beta.$$

(ii) Computation of the integral of B

$$B = -\int_0^{\theta_{\mathrm{m}}} f(\theta, \beta)(\cos\eta\theta\cos\beta\cos\theta + \sin\eta\theta\sin\theta)\mathrm{d}\theta$$

$$= -\cos\beta\int_0^{\theta_{\mathrm{m}}}\cos(\eta\theta)\cos\theta\mathrm{d}\theta - \int_0^{\theta_{\mathrm{m}}}\sin(\eta\theta)\sin\theta\mathrm{d}\theta$$

$$- \cos\beta\int_0^{\theta_{\mathrm{m}}}\cos(2\xi\beta\theta)\cos(\eta\theta)\cos\theta\mathrm{d}\theta$$

$$- \int_0^{\theta_{\mathrm{m}}}\cos(2\xi\beta\theta)\sin(\eta\theta)\sin\theta\mathrm{d}\theta$$

where the integrals of $\int_0^{\theta_{\mathrm{m}}}\cos(\eta\theta)\cos\theta\mathrm{d}\theta$, $\int_0^{\theta_{\mathrm{m}}}\sin(\eta\theta) \cdot \sin\theta\mathrm{d}\theta$, $\int_0^{\theta_{\mathrm{m}}}\cos(2\xi\beta\theta)\cos(\eta\theta)\cos\theta\mathrm{d}\theta$, and $\int_0^{\theta_{\mathrm{m}}}\cos \cdot (2\xi\beta\theta)\sin(\eta\theta)\sin\theta\mathrm{d}\theta$ are respectively

$$\int_0^{\theta_{\mathrm{m}}}\cos(\eta\theta)\cos\theta\mathrm{d}\theta$$

$$= \frac{1}{2}\int_0^{\theta_{\mathrm{m}}}\left[\cos(\eta\theta - \theta) + \cos(\eta\theta + \theta)\right]\mathrm{d}\theta$$

$$= \frac{1}{2} \cdot \frac{1}{\eta - 1} \cdot \sin(\eta\theta_{\mathrm{m}} - \theta_{\mathrm{m}}) + \frac{1}{2} \cdot \frac{1}{\eta + 1} \cdot \sin(\eta\theta_{\mathrm{m}} + \theta_{\mathrm{m}})$$

$$= -\frac{1}{2} \cdot \frac{1}{\eta - 1} \cdot \cos\left(\varphi - \frac{\pi}{2}\eta - \varphi\eta\right) + \frac{1}{2} \cdot \frac{1}{\eta + 1} \cdot \cos\left(\varphi + \frac{\pi}{2}\eta + \varphi\eta\right)$$

and

$$\int_0^{\theta_{\mathrm{m}}}\sin(\eta\theta)\sin\theta\mathrm{d}\theta = \frac{1}{2}\int_0^{\theta_{\mathrm{m}}}\left[\cos(\eta\theta - \theta) - \cos(\eta\theta + \theta)\right]\mathrm{d}\theta$$

$$= \frac{1}{2} \cdot \frac{1}{\eta - 1} \cdot \sin(\eta\theta_{\mathrm{m}} - \theta_{\mathrm{m}}) - \frac{1}{2} \cdot \frac{1}{\eta + 1} \cdot \sin(\eta\theta_{\mathrm{m}} + \theta_{\mathrm{m}})$$

$$= -\frac{1}{2} \cdot \frac{1}{\eta - 1} \cdot \cos\left(\varphi - \frac{\pi}{2}\eta - \eta\varphi\right) - \frac{1}{2} \cdot \frac{1}{\eta + 1} \cdot \cos\left(\varphi + \frac{\pi}{2}\eta + \eta\varphi\right)$$

and

$$\int_0^{\theta_{\mathrm{m}}}\cos(2\xi\beta\theta)\cos(\eta\theta)\cos\theta\mathrm{d}\theta$$

$$= \frac{1}{2}\int_0^{\theta_{\mathrm{m}}}\cos(2\xi\beta\theta)\left[\cos(\eta\theta - \theta) + \cos(\eta\theta + \theta)\right]\mathrm{d}\theta$$

$$= \frac{1}{2}\int_0^{\theta_{\mathrm{m}}}\cos(2\xi\beta\theta)\cos(\eta\theta - \theta)\mathrm{d}\theta$$

$$+ \frac{1}{2}\int_0^{\theta_{\mathrm{m}}}\cos(2\xi\beta\theta)\cos(\eta\theta + \theta)\mathrm{d}\theta$$

$$= \frac{1}{4}\int_0^{\theta_{\mathrm{m}}}\left[\cos(2\xi\beta\theta - (\eta\theta - \theta)) + \cos(2\xi\beta\theta + (\eta\theta - \theta))\right]\mathrm{d}\theta$$

$$+ \frac{1}{4}\int_0^{\theta_{\mathrm{m}}}\left[\cos(2\xi\beta\theta - (\eta\theta + \theta)) + \cos(2\xi\beta\theta + (\eta\theta + \theta))\right]\mathrm{d}\theta$$

$$= \frac{1}{4} \cdot \frac{1}{2\xi\beta - \eta + 1} \cdot \sin(2\xi\beta\theta_{\mathrm{m}} - \eta\theta_{\mathrm{m}} + \theta_{\mathrm{m}})$$

$$+ \frac{1}{4} \cdot \frac{1}{2\xi\beta + \eta - 1} \cdot \sin(2\xi\beta\theta_{\mathrm{m}} + \eta\theta_{\mathrm{m}} - \theta_{\mathrm{m}})$$

$$+ \frac{1}{4} \cdot \frac{1}{2\xi\beta - \eta - 1} \cdot \sin(2\xi\beta\theta_{\mathrm{m}} - \eta\theta_{\mathrm{m}} - \theta_{\mathrm{m}})$$

$$+ \frac{1}{4} \cdot \frac{1}{2\xi\beta + \eta + 1} \cdot \sin(2\xi\beta\theta_{\mathrm{m}} + \eta\theta_{\mathrm{m}} + \theta_{\mathrm{m}})$$

$$= \frac{1}{4} \cdot \frac{1}{2\xi\beta - \eta + 1} \cdot \cos\left[2\xi\beta\left(\frac{\pi}{2} + \varphi\right) - \eta\left(\frac{\pi}{2} + \varphi\right) + \varphi\right]$$

$$- \frac{1}{4} \cdot \frac{1}{2\xi\beta + \eta - 1} \cdot \cos\left[-2\xi\beta\left(\frac{\pi}{2} + \varphi\right) - \eta\left(\frac{\pi}{2} + \varphi\right) + \varphi\right]$$

$$- \frac{1}{4} \cdot \frac{1}{2\xi\beta - \eta - 1} \cdot \cos\left[-2\xi\beta\left(\frac{\pi}{2} + \varphi\right) + \eta\left(\frac{\pi}{2} + \varphi\right) + \varphi\right]$$

$$+ \frac{1}{4} \cdot \frac{1}{2\xi\beta + \eta + 1} \cdot \cos\left[2\xi\beta\left(\frac{\pi}{2} + \varphi\right) + \eta\left(\frac{\pi}{2} + \varphi\right) + \varphi\right]$$

and

$$\int_0^{\theta_{\mathrm{m}}}\cos(2\xi\beta\theta)\sin\eta\theta\sin\theta\mathrm{d}\theta$$

$$= \frac{1}{2}\int_0^{\theta_{\mathrm{m}}}\cos(2\xi\beta\theta)\left[\cos(\eta\theta - \theta) - \cos(\eta\theta + \theta)\right]\mathrm{d}\theta$$

$$= \frac{1}{2}\int_0^{\theta_{\mathrm{m}}}\cos(2\xi\beta\theta)\cos(\eta\theta - \theta)\mathrm{d}\theta$$

$$- \frac{1}{2}\int_0^{\theta_{\mathrm{m}}}\cos(2\xi\beta\theta)\cos(\eta\theta + \theta)\mathrm{d}\theta$$

$$= \frac{1}{4}\int_0^{\theta_{\mathrm{m}}}\left[\cos(2\xi\beta\theta - (\eta\theta - \theta)) + \cos(2\xi\beta\theta + (\eta\theta - \theta))\right]\mathrm{d}\theta$$

$$- \frac{1}{4}\int_0^{\theta_{\mathrm{m}}}\left[\cos(2\xi\beta\theta - (\eta\theta + \theta)) + \cos(2\xi\beta\theta + (\eta\theta + \theta))\right]\mathrm{d}\theta$$

$$= \frac{1}{4} \cdot \frac{1}{2\xi\beta - \eta + 1} \cdot \sin(2\xi\beta\theta_{\mathrm{m}} - \eta\theta_{\mathrm{m}} + \theta_{\mathrm{m}})$$

$$+ \frac{1}{4} \cdot \frac{1}{2\xi\beta + \eta - 1} \cdot \sin(2\xi\beta\theta_{\mathrm{m}} + \eta\theta_{\mathrm{m}} - \theta_{\mathrm{m}})$$

$$- \frac{1}{4} \cdot \frac{1}{2\xi\beta - \eta - 1} \cdot \sin(2\xi\beta\theta_{\mathrm{m}} - \eta\theta_{\mathrm{m}} - \theta_{\mathrm{m}})$$

$$- \frac{1}{4} \cdot \frac{1}{2\xi\beta + \eta + 1} \cdot \sin(2\xi\beta\theta_{\mathrm{m}} + \eta\theta_{\mathrm{m}} + \theta_{\mathrm{m}})$$

$$= \frac{1}{4} \cdot \frac{1}{2\xi\beta - \eta + 1} \cdot \cos\left[2\xi\beta\left(\frac{\pi}{2} + \varphi\right) - \eta\left(\frac{\pi}{2} + \varphi\right) + \varphi\right]$$

$$- \frac{1}{4} \cdot \frac{1}{2\xi\beta + \eta - 1} \cdot \cos\left[-2\xi\beta\left(\frac{\pi}{2} + \varphi\right) - \eta\left(\frac{\pi}{2} + \varphi\right) + \varphi\right]$$

$$+ \frac{1}{4} \cdot \frac{1}{2\xi\beta - \eta - 1} \cdot \cos\left[-2\xi\beta\left(\frac{\pi}{2} + \varphi\right) + \eta\left(\frac{\pi}{2} + \varphi\right) + \varphi\right]$$

$$- \frac{1}{4} \cdot \frac{1}{2\xi\beta + \eta + 1} \cdot \cos\left[2\xi\beta\left(\frac{\pi}{2} + \varphi\right) + \eta\left(\frac{\pi}{2} + \varphi\right) + \varphi\right].$$

Substituting the integrals of $\int_0^{\theta_m} \cos(\eta\theta)\cos\theta\,\mathrm{d}\theta$, $\int_0^{\theta_m} \sin(\eta\theta)\sin\theta\,\mathrm{d}\theta$, $\int_0^{\theta_m} \cos(2\xi\beta\theta)\cos(\eta\theta)\cos\theta\,\mathrm{d}\theta$, and $\int_0^{\theta_m} \cos(2\xi\beta\theta)\sin(\eta\theta)\sin\theta\,\mathrm{d}\theta$ into B, we obtained

$$
\begin{aligned}
B &= \frac{1}{2}\cdot\frac{\cos\beta+1}{\eta-1}\cdot\cos\left[\varphi-\left(\frac{\pi}{2}\eta+\varphi\eta\right)\right] \\
&+ \frac{1}{2}\cdot\frac{1-\cos\beta}{\eta+1}\cdot\cos\left[\varphi+\left(\frac{\pi}{2}\eta+\varphi\eta\right)\right] \\
&- \frac{1}{4}\left[\frac{\cos\beta+1}{2\xi\beta-\eta+1}\cdot\cos\left[\varphi-(\eta-2\xi\beta)\left(\frac{\pi}{2}+\varphi\right)\right]\right. \\
&- \frac{\cos\beta-1}{2\xi\beta-\eta-1}\cdot\cos\left[\varphi+(\eta-2\xi\beta)\left(\frac{\pi}{2}+\varphi\right)\right] \\
&+ \frac{\cos\beta-1}{2\xi\beta+\eta+1}\cdot\cos\left[\varphi+(2\xi\beta+\eta)\left(\frac{\pi}{2}+\varphi\right)\right] \\
&- \left.\frac{\cos\beta+1}{2\xi\beta+\eta-1}\cdot\cos\left[\varphi-(2\xi\beta+\eta)\left(\frac{\pi}{2}+\varphi\right)\right]\right] \\
&= \frac{\eta+\cos\beta}{\eta^2-1}\cdot\cos\varphi\cos\left(\frac{\pi}{2}\eta+\varphi\eta\right) \\
&+ \frac{\eta\cos\beta+1}{\eta^2-1}\cdot\sin\varphi\sin\left(\frac{\pi}{2}\eta+\varphi\eta\right) \\
&- \frac{1}{2}\left[\frac{\cos\beta-2\xi\beta+\eta}{1-(2\xi\beta-\eta)^2}\cdot\cos\varphi\cos\frac{(\eta-2\xi\beta)(\pi+2\varphi)}{2}\right. \\
&+ \frac{\eta\cos\beta-2\xi\beta\cos\beta+1}{1-(2\xi\beta-\eta)^2}\cdot\sin\varphi\sin\frac{(\eta-2\xi\beta)(\pi+2\varphi)}{2} \\
&+ \frac{\cos\beta+2\xi\beta+\eta}{1-(2\xi\beta+\eta)^2}\cdot\cos\varphi\cos\frac{(\eta+2\xi\beta)(\pi+2\varphi)}{2} \\
&+ \left.\frac{\eta\cos\beta+2\xi\beta\cos\beta+1}{1-(2\xi\beta+\eta)^2}\cdot\sin\varphi\sin\frac{(\eta+2\xi\beta)(\pi+2\varphi)}{2}\right].
\end{aligned}
$$

(iii) Computation of the integral of C

$$
\begin{aligned}
C &= \cos\beta\int_0^{\theta_m} f(\theta,\beta)\,\mathrm{d}\theta \\
&= \cos\beta\int_0^{\theta_m} 1\,\mathrm{d}\theta + \cos\beta\int_0^{\theta_m} \cos(2\xi\beta\theta)\,\mathrm{d}\theta \\
&= \theta_m\cos\beta + \frac{\cos\beta\sin(2\xi\beta\theta_m)}{2\xi\beta} \\
&= \left[\frac{\pi}{2}+\varphi+\frac{\sin(\pi\xi\beta+2\xi\beta\varphi)}{2\xi\beta}\right]\cos\beta.
\end{aligned}
$$

(iv) Computation of the integral of D

$$
\begin{aligned}
D &= \sin\beta\int_0^{\theta_m}\left(f(\theta,\beta)\cdot\cos(\eta\theta)\right)\mathrm{d}\theta \\
&= \sin\beta\int_0^{\theta_m}\cos(\eta\theta)\,\mathrm{d}\theta + \sin\beta\int_0^{\theta_m}\cos(2\xi\beta\theta)\cos(\eta\theta)\,\mathrm{d}\theta \\
&= \frac{\sin\beta}{\eta}\sin\left(\frac{\pi\eta}{2}+\varphi\eta\right) + \sin\beta\int_0^{\theta_m}\cos(2\xi\beta\theta)\cos(\eta\theta)\,\mathrm{d}\theta,
\end{aligned}
$$

where the integral of $\int_0^{\theta_m}\cos(2\xi\beta\theta)\cos(\eta\theta)\,\mathrm{d}\theta$ is

$$
\begin{aligned}
&\int_0^{\theta_m}\cos(2\xi\beta\theta)\cos(\eta\theta)\,\mathrm{d}\theta \\
&= \frac{1}{2}\int_0^{\theta_m}\left[\cos(2\xi\beta\theta-\eta\theta)+\cos(2\xi\beta\theta+\eta\theta)\right]\mathrm{d}\theta \\
&= \frac{1}{2}\cdot\frac{\sin(2\xi\beta\theta_m-\eta\theta_m)}{2\xi\beta-\eta}+\frac{1}{2}\cdot\frac{\sin(2\xi\beta\theta_m+\eta\theta_m)}{2\xi\beta+\eta} \\
&= \frac{1}{2\eta-4\xi\beta}\cdot\sin\frac{(\eta-2\xi\beta)(\pi+2\varphi)}{2} \\
&+ \frac{1}{2\eta+4\xi\beta}\cdot\sin\frac{(\eta+2\xi\beta)(\pi+2\varphi)}{2}.
\end{aligned}
$$

Substituting the integral of $\int_0^{\theta_m}\cos(2\xi\beta\theta)\cos(\eta\theta)\,\mathrm{d}\theta$ into D, we obtained

$$
\begin{aligned}
D &= \left[\frac{\sin\beta}{\eta}\cdot\sin\left(\frac{\pi\eta}{2}+\varphi\eta\right)\right] \\
&+ \sin\beta\left[\frac{1}{2\eta-4\xi\beta}\cdot\sin\frac{(\eta-2\xi\beta)(\pi+2\varphi)}{2}\right. \\
&+ \left.\frac{1}{2\eta+4\xi\beta}\cdot\sin\frac{(\eta+2\xi\beta)(\pi+2\varphi)}{2}\right] \\
&= \left[\frac{1}{\eta}\cdot\sin\left(\frac{\pi\eta}{2}+\varphi\eta\right)+\frac{1}{2\eta-4\xi\beta}\cdot\sin\frac{(\eta-2\xi\beta)(\pi+2\varphi)}{2}\right. \\
&+ \left.\frac{1}{2\eta+4\xi\beta}\cdot\sin\frac{(\eta+2\xi\beta)(\pi+2\varphi)}{2}\right]\sin\beta.
\end{aligned}
$$

References

[1] Briscoe B J, Sinha S K. Scratch resistance and localised damage characteristics of polymer surfaces-a review. *Materialwiss Werkst* **34**(10–11): 989–1002 (2003)

[2] Jiang H, Browning R, Sue H-J. Understanding of scratch-induced damage mechanisms in polymers. *Polymer* **50**(16): 4056–4065 (2009)

[3] Dasari A, Yu Z-Z, Mai Y-W. Fundamental aspects and recent progress on wear/scratch damage in polymer nanocomposites. *Mat Sci Eng R* **63**(2): 31–80 (2009)

[4] Brostow W, Deborde J, Jaclewicz M, Olszynski P. Tribology with emphasis on polymers: friction, scratch resistance and wear. *J Mater Educ* **24**(4–6): 119–132 (2003)

[5] Jiang H, Cheng Q, Jiang C, Zhang J, Li Y. Effect of stick-slip on the scratch performance of polypropylene. *Tribol Int* **91**: 1–5 (2015)

[6] Barr C J, Wang L, Coffey J K, Daver F. Influence of surface texturing on scratch/mar visibility for polymeric materials: a review. *J Mater Sci* **52**(3): 1221–1234 (2017)

[7] Moghbelli E, Sun L, Jiang H, Boo W J, Sue H J. Scratch behavior of epoxy nanocomposites containing α-zirconium phosphate and core–shell rubber particles. *Polym Eng Sci* **49**(3): 483–490 (2009)

[8] Misra R, Hadal R, Duncan S. Surface damage behavior during scratch deformation of mineral reinforced polymer composites. *Acta Mater* **52**(14): 4363–4376 (2004)

[9] Briscoe B J, Evans P D, Pellilo E, Sinha S K. Scratching maps for polymers. *Wear* **200**(1): 137–147 (1996)

[10] An J, Kang B-H, Choi B-H, Kim H-J. Observation and evaluation of scratch characteristics of injection-molded poly(methyl methacrylate) toughened by acrylic rubbers. *Tribol Int* **77**: 32–42 (2014)

[11] Zhang J, Jiang H, Jiang C, Cheng Q, Kang G. In-situ observation of temperature rise during scratch testing of poly(methylmethacrylate) and polycarbonate. *Tribol Int* **95**: 1–4 (2016)

[12] Barr C J, Wang L, Coffey J K, Gidley A, Daver F. New technique for the quantification of scratch visibility on polymeric textured surfaces. *Wear* **384–385**: 84–94 (2017)

[13] Hossain M M, Jahnke E, Boeckmann P, Guriyanova S, Minkwitz R, Sue H-J. Effect of thermal history on scratch behavior of multi-phase styrenic-based copolymers. *Tribol Int* **99**: 248–257 (2016)

[14] Wee J-W, Park S-Y, Choi B-H. Observation and understanding of scratch behaviors of glass fiber reinforced polycarbonate plates with various packing pressures during the injection molding process. *Tribol Int* **90**: 491–501 (2015)

[15] Jiang H, Lim G, Reddy J, Whitcomb J, Sue H J. Finite element method parametric study on scratch behavior of polymers. *J Polym Sci Pol Phys* **45**(12): 1435–1447 (2007)

[16] Pelletier H, Gauthier C, Schirrer R. Influence of the friction coefficient on the contact geometry during scratch onto amorphous polymers. *Wear* **268**(9): 1157–1169 (2010)

[17] Hossain M M, Jiang H, Sue H-J. Effect of constitutive behavior on scratch visibility resistance of polymers—A finite element method parametric study. *Wear* **270**(11): 751–759 (2011)

[18] Hossain M M, Browning R, Minkwitz R, Sue H-J. Effect of asymmetric constitutive behavior on scratch-induced deformation of polymers. *Tribol Lett* **47**(1): 113–122 (2012)

[19] Van Breemen L, Govaert L, Meijer H. Scratching polycarbonate: A quantitative model. *Wear* **274**: 238–247 (2012)

[20] Aleksy N, Kermouche G, Vautrin A, Bergheau J-M. Numerical study of scratch velocity effect on recovery of viscoelastic–viscoplastic solids. *Int J Mech Sci* **52**(3): 455–463 (2010)

[21] Felder E, Bucaille J L. Mechanical analysis of the scratching of metals and polymers with conical indenters at moderate and large strains. *Tribol Int* **39**(2): 70–87 (2006)

[22] Gao W M, Wang L, Coffey J K, Daver F. Understanding the scratch behaviour of polymeric materials with surface texture. *Materials & Design* **146**: 38–48 (2018)

[23] Feng B. Tribology behavior on scratch tests: Effects of yield strength. *Friction* **5**(1): 108–114 (2017)

[24] Feng B, Chen Z. Tribology behavior during indentation and scratch of thin films on substrates: effects of plastic friction. *AIP Advances* **5**(5): 057152 (2015)

[25] Subhash G, Zhang W. Investigation of the overall friction coefficient in single-pass scratch test. *Wear* **252**(1): 123–134 (2002)

[26] Lafaye S, Gauthier C, Schirrer R. A surface flow line model of a scratching tip: apparent and true local friction coefficients. *Tribol Int* **38**(2): 113–127 (2005)

[27] Lafaye S, Gauthier C, Schirrer R. Analysis of the apparent friction of polymeric surfaces. *J Mater Sci* **41**(19): 6441–6452 (2006)

[28] Lafaye S, Gauthier C, Schirrer R. Analyzing friction and scratch tests without in situ observation. *Wear* **265**(5): 664–673 (2008)

[29] Komvopoulos K. Sliding friction mechanisms of boundary-lubricated layered surfaces: Part II—Theoretical analysis. *Tribol T* **34**(2): 281–291 (1991)

[30] Jardret V, Zahouani H, Loubet J-L, Mathia T. Understanding and quantification of elastic and plastic deformation during a scratch test. *Wear* **218**(1): 8–14 (1998)

[31] Tayebi N, Conry T F, Polycarpou A A. Determination of hardness from nanoscratch experiments: Corrections for interfacial shear stress and elastic recovery. *J Mater Res* **18**(09): 2150–2162 (2003)

[32] Briscoe B, Biswas S, Sinha S, Panesar S. The scratch hardness and friction of a soft rigid-plastic solid. *Tribol Int* **26**(3): 183–193 (1993)

[33] Gauthier C, Lafaye S, Schirrer R. Elastic recovery of a scratch in a polymeric surface: experiments and analysis. *Tribol Int* **34**(7): 469–479 (2001)

[34] Pelletier H, Durier A-L, Gauthier C, Schirrer R. Viscoelastic and elastic–plastic behaviors of amorphous polymeric surfaces during scratch. *Tribol Int* **41**(11): 975–984 (2008)

[35] Bucaille J, Felder E, Hochstetter G. Mechanical analysis of the scratch test on elastic and perfectly plastic materials with the three-dimensional finite element modeling. *Wear* **249**(5): 422–432 (2001)

[36] Goddard J, Wilman H. A theory of friction and wear during the abrasion of metals. *Wear* **5**(2): 114–135 (1962)

[37] Lafaye S, Gauthier C, Schirrer R. The ploughing friction: analytical model with elastic recovery for a conical tip with a blunted spherical extremity. *Tribol Lett* **21**(2): 95–99 (2006)

[38] Lafaye S. True solution of the ploughing friction coefficient with elastic recovery in the case of a conical tip with a blunted spherical extremity. *Wear* **264**(7): 550–554 (2008)

[39] Ducret S, Pailler-Mattei C, Jardret V, Vargiolu R, Zahouani H. Friction characterisation of polymers abrasion (UHWMPE) during scratch tests: single and multi-asperity contact. *Wear* **255**(7): 1093–1100 (2003)

[40] Young D F, Munson B R, Okiishi T H, Huebsch W W. A brief introduction to fluid mechanics. John Wiley & Sons, 2010.

[41] Xiong D, Ge S. Friction and wear properties of UHMWPE/Al₂O₃ ceramic under different lubricating conditions. *Wear* **250**(1–12): 242–245 (2001)

[42] Tong J, Ma Y, Jiang M. Effects of the wollastonite fiber modification on the sliding wear behavior of the UHMWPE composites. *Wear* **255**(1–6): 734–741 (2003)

[43] Zoo Y-S, An J-W, Lim D-P, Lim D-S. Effect of Carbon Nanotube Addition on Tribological Behavior of UHMWPE. *Tribol Lett* **16**(4): 305–309 (2004)

[44] Pan D, Kang G, Jiang H. Viscoelastic constitutive model for uniaxial time-dependent ratcheting of polyetherimide polymer. *Polym Eng Sci* **52**(9): 1874–1881 (2012)

[45] Jiang H, Zhang J, Kang G, Xi C, Jiang C, Liu Y. A test procedure for separating viscous recovery and accumulated unrecoverable deformation of polymer under cyclic loading. *Polym Test* **32**(8): 1445–1451 (2013)

[46] Jiang C K, Jiang H, Zhang J W, Kang G Z. A viscoelastic–plastic constitutive model for uniaxial ratcheting behaviors of polycarbonate. *Polym Eng Sci* **55**(11): 2559–2565 (2015)

[47] Brostow W, Hagg Lobland H E, Narkis M. Sliding wear, viscoelasticity, and brittleness of polymers. *J Mater Res* **21**(9): 2422–2428 (2006)

[48] Brostow W, Kovacevic V, Vrsaljko D, Whitworth J. Tribology of polymers and polymer-based composites. *J Mater Educ* **32**(89): 273–290 (2010)

[49] Kalogeras I M, Hagg Lobland H E. The Nature of the Glassy State: Structure and Glass Transitions. *J Mater Educ* **34**(3–4): 69–94 (2012)

Chengkai JIANG. He received his bachelor degree in engineering mechanics from Southwest Jiaotong University, China, in 2012. After then, he was a PhD student at the same university. His research interests include polymer scratch and polymer constitutive modeling.

Han JIANG. He is a professor of the School of Mechanics and Engineering at Southwest Jiaotong University, China. He received his PhD degree in mechanical engineering from Texas A&M University in 2009. His research areas cover polymer scratch behaviors, and experimental investigation and constitutive modeling of polymeric materials.